

1 **Genetic drift versus regional spreading dynamics of COVID-19**

2

3 R. Di Pietro ¹, M. Basile ¹, L. Antolini ² and S. Alberti ³ *

4

5 ¹ Department of Medicine and Aging Sciences, Section of Biomorphology, G. d'Annunzio University
6 of Chieti-Pescara, Italy.

7 ² Center for Biostatistics, Department of Clinical Medicine, Prevention and Biotechnology,
8 University of Milano-Bicocca, Monza, Italy.

9 ³ Unit of Medical Genetics, Department of Biomedical Sciences - BIOMORF, University of Messina,
10 via Consolare Valeria, Messina, Italy.

11

12 * Address reprint requests to Prof. Alberti at the Unit of Medical Genetics, Department of Biomedical
13 Sciences - BIOMORF, University of Messina, via Consolare Valeria, Messina, Italy, or at
14 salberti@unime.it

15

16 Drs. Di Pietro and Basile contributed equally to this article.

17

18

19 **Running title:** COVID-19 diffusion rate determinants

20

21 **Word count of the abstract:** 236

22

23 **Word count of the text:** 2,472

24 **Abstract**

25 **Background**

26 Current propagation models of COVID-19 pandemic spreading appear poorly consistent with existing
27 epidemiological data and with evidence that SARS-CoV-2 is rapidly mutating, for potential
28 aggressive evolution of the disease.

29 **Methods**

30 We thus challenged environmental versus genetic evolution models of COVID-19 spreading, in the
31 largest epidemiological analysis conducted as yet. This was performed over 168,089 laboratory-
32 confirmed infection cases in Italy, Spain and Scandinavia. Landmark dates were set for each of the
33 countries analyzed at peak diffusion rates this date, and the doubling time versus cumulative number
34 of diagnoses was computed. Diffusion data in Germany, France and UK constituted the validation
35 dataset of our model, over 210,239 additional cases. Mutations and mutation rates of SARS-CoV-2
36 versus COVID-19 spreading were analyzed at nextstrain.org/ncov/europe.

37 **Results**

38 The mean doubling time of COVID-19 was 6.63 days in northern Italy, 5.87 days in central areas,
39 and 5.38 days in southern Italy, for shorter COVID-19 doubling time in warmer regions. Spain
40 extended this trend, with a mean COVID-19 doubling time of 4.2 days. Slower diffusion across
41 progressively colder regions was observed in Scandinavia, with 9.4 days COVID-19 doubling time
42 in Sweden, 10.8 days in Finland and 12.95 days in Norway. Such diffusion model was supported by
43 SARS-CoV-2 mutation strings upon sequential diffusion across the North/South gradient.

44 **Conclusions**

45 Our findings indicate COVID-19 association to a sharp North/South climate gradient, with faster
46 spreading in southern regions. Thus, warmer climate conditions may not limit SARS-CoV-2
47 diffusion. Very cold regions may be better spared by recurrent courses of SARS-CoV-2 infection.

48

49

50 **Keywords:** COVID-19, pandemic, spreading dynamics, climate areas, mutation rates.

51 **Introduction**

52 A first study on 425 cases identified initial transmission dynamics of Severe Acute Respiratory
53 Syndrome (SARS) in 2019 (COVID-19) in China (1). In its early stages, the epidemic doubled in
54 size every 6.4 (2) to 7.4 (1) days, with a reproductive number (R_0) of infectious cases from 2.2 (1) to
55 2.7 (2). Later studies described how the disease spread to Singapore (3), then to Germany (4), France
56 and Finland (www.ecdc.europa.eu/en/covid-19-pandemic) (5-7).

57 However, key epidemiological evidence remained to be acquired (7). Major uncertainties
58 remained on COVID-19 spreading determinants. SARS-CoV-2 was proposed to be sensitive to
59 temperature and humidity, which may affect diffusion across diverse climate areas (8)
60 (papers.ssrn.com/sol3/papers.cfm?abstract_id=3550308; ssrn.com/abstract=3556998;
61 www.medrxiv.org/content/10.1101/2020.02.22.20025791v1). Diversity among substrains of SARS-
62 CoV-2 occurs across different regions in the world (nextstrain.org/ncov/global). SARS-CoV-2
63 possesses a single-strand RNA genome (9) and was soon found to acquire genomic mutations.
64 Selective pressure may apply to SARS-CoV-2 genomic drifting, and this may cooperatively drive
65 geographic diffusion.

66 Current propagation models predicted a limited impact of COVID-19 in the Southern
67 hemisphere during seasons that were infection-prone in the Northern hemisphere
68 (papers.ssrn.com/sol3/papers.cfm?abstract_id=3550308; ssrn.com/abstract=3556998). However,
69 early foci of infection were detected in Australia and New Zealand (Figure 1). Outbreaks were also
70 revealed in South America and extended to Central America and Mexico. Further infection foci were
71 revealed in Saudi Arabia and Africa, and extended to sub-Saharan countries (Tables S1, S2),
72 questioning simple models of climate-dependent COVID-19 spreading. Coronaviruses spread to
73 some extent similarly to the influenza virus (8), through small droplets suspended in the air,
74 suggesting sensitivity to environmental humidity and temperature conditions. A recent meta-analysis
75 (10), though, indicated resilience of coronaviruses to the environment. In a comparison to SARS-
76 CoV-1, SARS-CoV-2 remained viable in aerosols for hours, and persisted over solid surfaces, 72
77 hours on plastic, 48 hours on stainless steel and 24 hours on cardboard (11), raising issues on current
78 SARS-CoV-2 diffusion models.

79 This led us to challenge a genetic versus climate-driven additive coronavirus infection model.
80 A robust analysis of SARS-CoV-2 spreading determinants required high-information density (12,
81 13). Case incidence models depend on complex factors interplay (global traveling, founder effect
82 versus time from initial infection (2), population clustering in big cities, social dynamics, infectious
83 ability of the virus (14, 15), COVID-19 containment procedures). Among them, a major confounding
84 factor is the time of initial infection at any given place, which, everything else being equal, leads to

85 vastly different absolute numbers of derived cases (2). Velocity of infection spreading had previously
86 been shown to be a hard composite index of the R_0 of the virus and of patients viral load/disease
87 stage/severity (1, 16) and is insensitive to the time of infection seeding. Hence, infection doubling
88 time was utilized as a COVID-19 descriptor in this study.

89 Vastly diverse climatic regions around the CET longitude (15°E), were severely exposed to
90 infection. Spain and Italy were the countries with the highest initial incidence of COVID-19 in Europe
91 (Figures 1, S1, Table S3). The heaviest initial casualties in Italy were suffered by Lombardy and
92 Veneto, i.e. cold and humid areas during wintertime. Markedly warmer and drier climate conditions
93 prevail in southern regions of the country. A further shift toward warmer/drier conditions occurs in
94 Spain. Scandinavian countries appeared initially spared by the infection (Table S4) and provided a
95 reference for cold winter temperatures, over a Sweden-Finland-Norway axis. Thus, we assessed a
96 climate-dependent coronavirus infection model, through a global-scale analysis of 86,498 infection
97 cases in Italy, 64,095 in Spain, versus 17,496 cases in Scandinavia ([github.com/pcm-dpc/COVID-](https://github.com/pcm-dpc/COVID-19)
98 [19](https://github.com/pcm-dpc/COVID-19)) (Supplemental Appendix). Diffusion data in France (Table S5), Germany (Table S6), and UK
99 (Table S7) were utilized as a validation dataset of 210,239 infection cases. This model was then
100 merged with the coronavirus genetic drift-driven diffusion determinants, according to mutation
101 trajectories in the analyzed areas.

102

103 **Methods**

104 **Incidence data**

105 Laboratory-confirmed infection cases in Europe cases were retrieved at peak diffusion rates as
106 follows: Italy (github.com/pcm-dpc/COVID-19, March 27th 2020), France
107 (dashboard.covid19.data.gouv.fr/vue-d-ensemble?location=FRA; April 4th 2020), UK
108 (www.nhs.uk/; April 9th 2020), Germany (corona.rki.de; April 2nd 2020), Spain (RTVE - Ministry of
109 Health; www.rtve.es/noticias/20200415/mapa-del-coronavirus-espana/2004681.shtml; March 31st
110 2020), Sweden (Public Health Agency of Sweden; [www.folkhalsomyndigheten.se/smittskydd-](https://www.folkhalsomyndigheten.se/smittskydd-beredskap/utbrott/aktuella-utbrott/covid-19)
111 [beredskap/utbrott/aktuella-utbrott/covid-19](https://www.folkhalsomyndigheten.se/smittskydd-beredskap/utbrott/aktuella-utbrott/covid-19); April 13th 2020), Finland (National Institute for Health
112 and Welfare THL; thl.fi/en/web/thlfi-en; April 7th 2020), Norway; data from the Norwegian Institute
113 of Public Health; [www.fhi.no/sv/smittsomme-sykdommer/corona/dags--og-ukerapporter/dags--og-](https://www.fhi.no/sv/smittsomme-sykdommer/corona/dags--og-ukerapporter/dags--og-ukerapporter-om-koronavirus)
114 [ukerapporter-om-koronavirus](https://www.fhi.no/sv/smittsomme-sykdommer/corona/dags--og-ukerapporter/dags--og-ukerapporter-om-koronavirus); April 7th 2020). All available data in each national registry were
115 systematically included in the analysis.

116 Incidence data were collapsed into a global database, to explore case incidence over time, and
117 health outcome measures across countries and country provinces. Disease severity was classified as
118 (a) hospitalized cases, (b) intensive-care unit patients, (c) recovered cases, (d) deaths. Incidence

119 scatter plots by region were linked to Köppen–Geiger climate classification maps (koeppen-geiger.vu-wien.ac.at/present.htm). These were computed as mean parametrization of 1980-2016 data
120 (17). The three-variable classification by country areas was quantified as a string and utilized as an
121 independent variable versus COVID-19 spreading velocity ([Table 1](#)).
122

123

124 **SARS-CoV-2 mutation analysis**

125 SARS-CoV-2 genomic RNA sequences and country-correlated data were obtained from
126 nextstrain.org/ncov/global. Scatter plots were generated, by strings of acquired mutations over time
127 and overall number of mutations per genome per chosen area. Phylogeny trees for compiled mutations
128 strings were then obtained according to mutant branch descriptors
129 (nextstrain.org/ncov/europe?branchLabel=aa) ([Figures S2-9](#)).
130

130

131 **Statistical analysis**

132 The cumulative incidence of COVID-19 diagnoses was contrasted to calendar time for each province
133 in a scatter plot (12, 13). These plots acted as a smoother, for determining the trajectory of infection
134 cases. A landmark date for total numbers of diagnoses was set according to case incidence shape in
135 each dataset. From this date, the doubling time for cumulative number of diagnoses was calculated
136 backward for each province as follows. Two dates were identified: the maximum date, at which the
137 cumulative number of diagnoses were lower than a half of the cumulative number of diagnoses at the
138 landmark time, and the minimum date, with a cumulative number of diagnoses greater than a half of
139 the cumulative number of diagnoses at the landmark date. The fraction of days from the
140 minimum date to achieve half of the cumulative number of diagnoses at the landmark date were
141 obtained by a linear assumption for the cumulative incidence between the two dates. Comparison of
142 doubling time values was conducted versus central intercepts. Coefficients, standard error, 95%
143 confidence intervals were computed. Percentile distribution boxplots of COVID-19 doubling times
144 were drawn. Median, maximum value, minimum value and distribution outliers were computed. The
145 correlation of discrete values of COVID-19 spreading rates curve versus climate-area string values
146 was computed by Anova.
147

147

148 **Software**

149 Stata software version 16 was used for data importing, manipulation and graphics (StataCorp.
150 2019. *Stata Statistical Software: Release 16*. College Station, TX: StataCorp LLC).
151

151

152 **Results**

153 Our attention was first drawn to the Southern hemisphere. Simple propagation models predicted
154 essential absence of COVID-19 diffusion, during seasons that were infection-prone in the Northern
155 hemisphere. However, early foci of infection were detected in Australia and New Zealand ([Figure](#)
156 [1A](#)). South and Central America appeared initially spared. Assessment at later time points indicated,
157 though, large-scale (≥ 30 infection cases) outbreaks in Argentina, Bolivia, Brazil, Chile, Colombia,
158 Ecuador, Perú, Uruguay, Venezuela. Parallel outbreaks were revealed in Costa Rica, Dominican
159 Republic, Panama and Mexico ([Figure 1C](#), [Table S1](#)).

160 Africa, Middle-East and the Arabian peninsula also appeared spared during the initial course
161 of COVID-19 ([Figure 1A](#)). However, infection foci appeared soon in Saudi Arabia, a non-high-risk
162 country by most standards. This was soon recognized as a risk for COVID-19 spreading (18), and
163 Saudi Arabia suspended the Umrah pilgrimage to Mecca and Medina on March 4th. Additional cases
164 were reported in United Arab Emirates, Bahrain, Kuwait, Oman. Infectious foci were revealed in
165 other countries facing the Persian Gulf and the Gulf of Oman, such as Iraq, Iran, Afghanistan,
166 Pakistan. Further outbreaks were recorded in continental Africa, i.e. in Algeria, Egypt, Burkina Faso,
167 Senegal, Democratic Republic of the Congo, Cameroon, Côte d'Ivoire, Ghana, Nigeria, South Africa
168 ([Table S2](#)).

169

170 **COVID-19 doubling time by geographic area**

171 We thus moved on to computing spreading rates of COVID-19 in compared areas in Europe. Global
172 data were collected from country registries and infection rates over time were computed for:

173 Italy: on infection cases from March 3rd to March 27th (n=86,498) ([Supplemental Appendix](#)) ([Figures](#)
174 [S10-12](#)).

175 Spain: on infection cases from February 25th to March 27th 2020 (n=64,095) ([Figure S13](#)).

176 Norway: data (>50 infection case outbreaks) were obtained from February 21st to April 14th 2020
177 (n=6,676) ([Figure S14](#)).

178 Finland: on infection cases from March 1st to April 7th 2020 (n=2,646) ([Figure S15](#)).

179 Sweden: data (>50 infection case outbreaks) were obtained from February 26th to April 9th 2020
180 (n=8,995) ([Figure S16](#)).

181 France: on infection cases from February 25th to April 4th 2020 ([Figure S17](#)).

182 UK: on infection cases from February 1st to April 9th 2020 ([Figure S17](#)).

183 Germany: on infection cases from February 24th to April 2nd 2020 ([Figure S17](#)).

184 COVID-19 doubling times by Countries, Regions and Provinces were computed as indicated.
185 Landmark dates were utilized as set for each analyzed geographic area. From this date the time for
186 doubling the cumulative number of diagnoses was calculated backward for each province.

187

188 **COVID-19 doubling time versus climate region**

189 Quantitative climate assessments are affected by interdependent sets of variables, such as humidity
190 and temperature, which provide sources of uncertainty in climate models (19). We thus utilized the
191 Köppen–Geiger climate classification maps (koeppen-geiger.vu-wien.ac.at/present.htm), as drawn
192 over 30+ years of observations. This was distilled as a three-variable classification by country areas,
193 quantified as a string and utilized as an independent variable versus COVID-19 spreading velocity
194 (Table 1).

195 Summary doubling times were grouped by geographic region. The average doubling time for
196 northern Italy was 6.63 (SD=1.94) days; 5.87 (SD=1.08) days in central regions; 5.38 (SD=2.31) days
197 in southern areas, for significantly shorter doubling time in southern regions ($P=0.02$) (Table S3,
198 Figures S10-12). The mean COVID-19 doubling-time for the whole country was 6.06 (SD=1.95)
199 days (Table S3).

200 With a doubling time of 4.2-days, Spain extended such an indication (Figure S13). At the
201 opposite end of the climate spectrum, Scandinavia showed longer COVID-19 doubling times, over a
202 Sweden-Finland-Norway axis, with a doubling time of 9.4 days (SD=1.2) for Sweden ($P<0.0001$
203 versus northern Italy), 10.8 days for Finland, 12.95 days (SD=0.52) for Norway ($P<0.0001$ versus
204 northern Italy) (Table S3, Figures S14-16). This depicted a distinct North-South gradient of COVID-
205 19 spreading velocity (Anova $P<0.0001$) (Table 1).

206 Such climate model was challenged versus COVID-19 diffusion rates in Germany, France
207 and UK over 210,239 laboratory-confirmed infection cases. Pandemic doubling time was computed
208 to be 7.0 days in Germany (Figure S17). In sharp consistency, those in France and UK were 7.5 and
209 7.2 days, respectively. Average climate areas for Germany, France and UK were Cfb Köppen–Geiger
210 climate classification classes (Table 1), which bridged classification classes of Northern Italy and
211 Southern Sweden, as predicted by the model.

212

213 **SARS-CoV-2 genetic-drift driven diffusion**

214 The SARS-CoV-2 genomic RNA was shown to progressively mutate over time
215 (nextstrain.org/ncov/europe). To determine whether mutation strings correlated with diffusion at
216 distinct geographic areas, SARS-CoV-2 genomic RNA sequences from different countries were
217 obtained at sequential times. Scatter plots were then generated, for strings of acquired mutations
218 versus overall number of accumulated mutations versus time. Phylogeny trees for compiled mutations
219 were then obtained, according to mutant clade descriptors
220 (nextstrain.org/ncov/europe?branchLabel=aa).

221 Sequence mutation analysis revealed up to seven major branches of linear mutation
222 acquisition, at sites of major diffusion after spreading from China (Figures S2-9). A mutation string-
223 driven aggressiveness of SARS-CoV-2 spreading, was predicted to lead to (a) correlation of specific
224 strings with hardest-hit countries, (b) a late predominance of one/few dominant strings over the course
225 of COVID-19 and (c) increase in disease severity over time. The highest numbers of accumulated
226 mutations were revealed in SARS-CoV-2 in Wales and Senegal isolates, which were identified as
227 late disease correlates. Consistent, the lowest number of accumulated mutations was recorded in Italy,
228 the country that was first to show strong disease severity in Europe. A large mutation load was
229 observed in Spain (n=14), the second hardest-hit country in Europe, as close to that of Sweden (n=13),
230 a country with much more limited COVID-19 diffusion. Large mutation loads in late-disease-
231 insurgence countries, such as France and Belgium (n=16), lend additional support to drive by duration
232 of disease course. Consistent, four major mutation strings branches were revealed in all examined
233 European countries, indicating dependence on specific substrains of SARS-CoV-2.

234

235 Discussion

236 Rapid COVID-19 diffusion in Southern hemisphere countries, such as Australia, New Zealand, South
237 and Central America, together with early infection outbreaks in Africa, Middle-East and in the
238 Arabian peninsula posed early questions on influenza-like propagation models of SARS-CoV-2.
239 Potent models were subsequently constructed that better took the complexity of COVID-19 diffusion
240 into account (19, 20). However, actual, high-dimensional data on COVID-19 infection dynamics
241 remained largely missing (7).

242 Our work provided the needed data to this end, as the largest epidemiological analysis of
243 COVID-19 diffusion conducted as yet. All available data from each national registry were
244 systematically included in the analysis, for over 378,328 laboratory-confirmed infection cases in
245 continental Europe and UK. This analysis was then merged with mutation-string-driven SARS-CoV-
246 2 spreading at distinct geographic areas.

247 Four major mutation strings branches were revealed in all examined European countries,
248 indicating relationship with specific substrains of SARS-CoV-2. The highest numbers of accumulated
249 mutations were revealed in SARS-CoV-2 in Wales and Senegal isolates, which were identified as
250 late disease correlates. The lowest number of accumulated mutations was recorded in Italy, the
251 country that was first to show severe disease outbreaks in Europe. A large mutation load was observed
252 in Spain, which followed as second hardest-hit country in Europe, as close to that of Sweden, a
253 country with late COVID-19 diffusion. The largest mutational loads were revealed in France and
254 Belgium, as late-disease-insurgence countries, further supporting intertwining with successive stages

255 of disease course.

256 We then found that COVID-19 spreading velocity followed a North-South gradient in Italy,
257 for significantly shorter doubling times in southern regions. With a doubling time of 4.2-days, Spain
258 extended such an indication. At the opposite end of the climate spectrum, Scandinavia showed longer
259 COVID-19 doubling times, over a Sweden-Finland-Norway axis, for a sharp, quantitative North-
260 South gradient of COVID-19 spreading velocity. This climate model was verified in validation
261 datasets of COVID-19 diffusion in Germany, France and UK over 210,239 laboratory-confirmed
262 infection cases. Pandemic doubling times were sharply consistent in Germany, France and UK,
263 according to ultimate climate-area Köppen–Geiger fingerprints, thus coordinately bridging Northern
264 Italy classes with Southern Sweden.

265 These results indicate significantly faster diffusion of COVID-19 in warmer regions. Such
266 findings are consistent with indications of resilience of coronaviruses to climate conditions (10) and
267 long-term viability of SARS-CoV-2 in the environment (11). Of note, the Middle East Respiratory
268 Syndrome (MERS) was first reported in Saudi Arabia (www.cdc.gov/coronavirus/mers). MERS
269 is caused by the MERS-CoV, which is structurally and genetically related to SARS-CoV. MERS is
270 endemic in the Arabic Peninsula, indicating that at least specific coronavirus strains are resilient to
271 desert climate conditions (www.cdc.gov/coronavirus/mers/risk.html).

272 Taken together, our findings suggest resilience of SARS-CoV-2 in warmer regions, and
273 caution that high environmental temperatures may not efficiently tame SARS-CoV-2 infectiousness
274 (20). On the other hand, very cold regions may be better spared by recurrent courses of COVID-19.

275

276 **Acknowledgments**

277 We are much indebted to all the information curators we cite, and to the website providers the article
278 data and graphic primers have been downloaded from.

279

280 **Role in the article**

281 All authors contributed to literature search, figures, study design, data collection, data analysis, data
282 interpretation. S.A and R.DiP. wrote the manuscript draft. All authors contributed to discussing and
283 writing the final text. R.DiP. and M.B. contributed equally to this work.

284

285 **Footnote page**

286 Conflict of interest

287 The authors do not have a commercial or other association that might pose a conflict of interest.

288

289 Funding

290 The University of Messina and Oncoxx Biotech srl provided funding to this work.

291

292 Meeting presentation

293 These findings have not yet been presented to meetings.

294

295 Corresponding author contact information

296 Prof. Saverio Alberti, Head, Medical Genetics, Department of Biomedical Sciences, University of

297 Messina, via Consolare Valeria, 98100 Messina, Italy, Phone: (+39) 090-221.3375, E-mail:

298 salberti@unime.it

299 **References**

- 300 1. Li Q, Guan X, Wu P, Wang X, Zhou L, Tong Y, Ren R, Leung KSM, Lau EHY, Wong JY, Xing
301 X, Xiang N, Wu Y, Li C, Chen Q, Li D, Liu T, Zhao J, Liu M, Tu W, Chen C, Jin L, Yang R, Wang
302 Q, Zhou S, Wang R, Liu H, Luo Y, Liu Y, Shao G, Li H, Tao Z, Yang Y, Deng Z, Liu B, Ma Z,
303 Zhang Y, Shi G, Lam TTY, Wu JT, Gao GF, Cowling BJ, Yang B, Leung GM, Feng Z. 2020.
304 Early Transmission Dynamics in Wuhan, China, of Novel Coronavirus-Infected
305 Pneumonia. *New England Journal of Medicine* 382:1199-1207.
- 306 2. Wu JT, Leung K, Leung GM. 2020. Nowcasting and forecasting the potential domestic and
307 international spread of the 2019-nCoV outbreak originating in Wuhan, China: a
308 modelling study. *The Lancet* 395:689-697.
- 309 3. Pung R, Chiew CJ, Young BE, Chin S, Chen MIC, Clapham HE, Cook AR, Maurer-Stroh S,
310 Toh MPHS, Poh C, Low M, Lum J, Koh VTJ, Mak TM, Cui L, Lin RVTP, Heng D, Leo Y-S, Lye
311 DC, Lee VJM, Kam K-q, Kalimuddin S, Tan SY, Loh J, Thoon KC, Vasoo S, Khong WX,
312 Suhaimi N-A, Chan SJH, Zhang E, Oh O, Ty A, Tow C, Chua YX, Chaw WL, Ng Y, Abdul-
313 Rahman F, Sahib S, Zhao Z, Tang C, Low C, Goh EH, Lim G, Hou Ya, Roshan I, Tan J, Foo K,
314 Nandar K, Kurupatham L, Chan PP, et al. 2020. Investigation of three clusters of COVID-
315 19 in Singapore: implications for surveillance and response measures. *The Lancet*
316 395:1039-1046.
- 317 4. Hoehl S, Rabenau H, Berger A, Kortenbusch M, Cinatl J, Bojkova D, Behrens P,
318 Böddinghaus B, Götsch U, Naujoks F, Neumann P, Schork J, Tiarks-Jungk P, Walczok A,
319 Eickmann M, Vehreschild MJGT, Kann G, Wolf T, Gottschalk R, Ciesek S. 2020. Evidence
320 of SARS-CoV-2 Infection in Returning Travelers from Wuhan, China. *New England*
321 *Journal of Medicine* 382:1278-1280.
- 322 5. Sun J, He W-T, Wang L, Lai A, Ji X, Zhai X, Li G, Suchard MA, Tian J, Zhou J, Veit M, Su S.
323 2020. COVID-19: Epidemiology, Evolution, and Cross-Disciplinary Perspectives. *Trends*
324 *in Molecular Medicine* doi:<https://doi.org/10.1016/j.molmed.2020.02.008>.
- 325 6. McMichael TM, Currie DW, Clark S, Pogosjans S, Kay M, Schwartz NG, Lewis J, Baer A,
326 Kawakami V, Lukoff MD, Ferro J, Brostrom-Smith C, Rea TD, Sayre MR, Riedo FX, Russell
327 D, Hiatt B, Montgomery P, Rao AK, Chow EJ, Tobolowsky F, Hughes MJ, Bardossy AC,
328 Oakley LP, Jacobs JR, Stone ND, Reddy SC, Jernigan JA, Honein MA, Clark TA, Duchin JS.
329 2020. Epidemiology of Covid-19 in a Long-Term Care Facility in King County,
330 Washington. *New England Journal of Medicine* doi:10.1056/NEJMoa2005412.
- 331 7. Lipsitch M, Swerdlow DL, Finelli L. 2020. Defining the Epidemiology of Covid-19 —
332 Studies Needed. *New England Journal of Medicine* 382:1194-1196.

- 333 8. Sundell N, Andersson L-M, Brittain-Long R, Lindh M, Westin J. 2016. A four year seasonal
334 survey of the relationship between outdoor climate and epidemiology of viral
335 respiratory tract infections in a temperate climate. *Journal of Clinical Virology* 84:59-63.
- 336 9. Mousavizadeh L, Ghasemi S. 2020. Genotype and phenotype of COVID-19: Their roles in
337 pathogenesis. *Journal of Microbiology, Immunology and Infection*
338 doi:<https://doi.org/10.1016/j.jmii.2020.03.022>.
- 339 10. Kampf G, Todt D, Pfaender S, Steinmann E. 2020. Persistence of coronaviruses on
340 inanimate surfaces and their inactivation with biocidal agents. *Journal of Hospital*
341 *Infection* 104:246-251.
- 342 11. van Doremalen N, Bushmaker T, Morris DH, Holbrook MG, Gamble A, Williamson BN,
343 Tamin A, Harcourt JL, Thornburg NJ, Gerber SI, Lloyd-Smith JO, de Wit E, Munster VJ.
344 2020. Aerosol and Surface Stability of SARS-CoV-2 as Compared with SARS-CoV-1. *New*
345 *England Journal of Medicine* doi:10.1056/NEJMc2004973.
- 346 12. Ambrogi F, Biganzoli E, Querezoli P, Ferretti S, Boracchi P, Alberti S, Marubini E, Nenci I.
347 2006. Molecular subtyping of breast cancer from traditional tumor marker profiles
348 using parallel clustering methods. *Clin Cancer Res* 12:781-90.
- 349 13. Cimoli G, Malacarne D, Ponassi R, Valenti M, Alberti S, Parodi S. 2004. Meta-analysis of
350 the role of p53 status in isogenic systems tested for sensitivity to cytotoxic
351 antineoplastic drugs. *Biochim Biophys Acta* 1705:103-20.
- 352 14. To KK-W, Tsang OT-Y, Leung W-S, Tam AR, Wu T-C, Lung DC, Yip CC-Y, Cai J-P, Chan JM-
353 C, Chik TS-H, Lau DP-L, Choi CY-C, Chen L-L, Chan W-M, Chan K-H, Ip JD, Ng AC-K, Poon
354 RW-S, Luo C-T, Cheng VC-C, Chan JF-W, Hung IF-N, Chen Z, Chen H, Yuen K-Y. 2020.
355 Temporal profiles of viral load in posterior oropharyngeal saliva samples and serum
356 antibody responses during infection by SARS-CoV-2: an observational cohort study. *The*
357 *Lancet Infectious Diseases* doi:[https://doi.org/10.1016/S1473-3099\(20\)30196-1](https://doi.org/10.1016/S1473-3099(20)30196-1).
- 358 15. Chen Y, Li L. 2020. SARS-CoV-2: virus dynamics and host response. *The Lancet Infectious*
359 *Diseases* doi:10.1016/S1473-3099(20)30235-8.
- 360 16. Liu Y, Eggo RM, Kucharski AJ. 2020. Secondary attack rate and superspreading events
361 for SARS-CoV-2. *The Lancet* 395:e47.
- 362 17. Beck HE, Zimmermann NE, McVicar TR, Vergopolan N, Berg A, Wood EF. 2018. Present
363 and future Köppen-Geiger climate classification maps at 1-km resolution. *Scientific data*
364 5:180214-180214.
- 365 18. Ebrahim SH, Memish ZA. 2020. COVID-19: preparing for superspreader potential among
366 Umrah pilgrims to Saudi Arabia. *The Lancet* 395:e48.

- 367 19. Baker RE, Yang W, Vecchi GA, Metcalf CJE, Grenfell BT. 2020. Susceptible supply limits
368 the role of climate in the early SARS-CoV-2 pandemic. Science
369 doi:10.1126/science.abc2535:eabc2535.
- 370 20. Kissler SM, Tedijanto C, Goldstein E, Grad YH, Lipsitch M. 2020. Projecting the
371 transmission dynamics of SARS-CoV-2 through the postpandemic period. Science
372 doi:10.1126/science.abb5793:eabb5793.
- 373

374 **Figure legends**

375

376 **Figure 1. Worldwide progression of COVID-19.**

377 (A) COVID-19 case incidence, as of 21st 2020; numbers are indicated by color code and circle
378 diameter (www.healthmap.org/covid-19/).

379 (B) COVID-19 case incidence, as in (A), zoomed over Central Europe.

380 (C) COVID-19 incidence of active cases, as of March 31st, 2020; numbers are indicated by circle
381 diameter (Johns Hopkins University, JHU; coronavirus.jhu.edu/map.html).

382 (D) Coronavirus spreading around the world as of April 4th. Confirmed cases by country since
383 February 24th (JHU, public.flourish.studio/visualisation/1694807/).

384

385 **Figure 2. COVID-19 diffusion and SARS-CoV-2 mutations.**

386 (A) SARS-CoV-2 virus spread according to mutation load.

387 (B) Radial diagram of SARS-CoV-2 mutations worldwide. Concentric circles correspond to the
388 number of genomic mutations detected in individual virus isolates.

389

390 **Figure 3. COVID-19 diffusion across geographic areas.**

391 (*top*) Distribution boxplots of COVID-19 doubling times. Upper horizontal line: 75th percentile; lower
392 horizontal line: 25th percentile; horizontal bar within box: median; upper horizontal bar outside box:
393 maximum value; lower horizontal bar outside box: minimum value. Dots: distribution outliers.

394 (*bottom*) doubling time values versus central intercept – Northern Italy. Coef.: coefficient; Std. Err.:
395 standard error; 95% confidence intervals are shown. P>t: 0.002 Southern versus Northern Italy;
396 <0.0001 Sweden versus Northern Italy; <0.0001 Norway versus Northern Italy.

397

398 **Figure 4. The COVID-19 North-South gradient.**

399 The COVID-19 North-South doubling-time gradient across countries by climate zone is depicted.

400 The Anova P-value for trend of the curve is shown. Vertical arrows: COVID-19 doubling times in
401 validation datasets (Germany, France, UK).

402

403 **Table 1: COVID-19 doubling time versus climate area.**

Country/region	COVID-19 doubling time (days)	Climate area	Lab-confirmed case numbers *
Spain	4.2	Csa/Csb/Bsk	64,095
Southern Italy	5.38	Csa/Csb	5,322
Central Italy	5.87	Csa/Cfa/Cfb	10,842
Northern Italy	6.63	Cfa/Cfb	70,334
Germany	7.0	Cfb	73,522
France	7.5	Cfb	68,665
UK	7.2	Cfb	68,052
Sweden	9.4	Dfc/Cfb	11,321
Finland	10.8	Dfc/Dfb	2,646
Norway	12.95	Dfc/Dfb/ET	5,855

404

405 *: Laboratory-confirmed infection cases in Europe cases were retrieved by country at peak diffusion rates as follows:
 406 Italy (github.com/pcm-dpc/COVID-19, March 27th 2020), France ([dashboard.covid19.data.gouv.fr/vue-d-](https://dashboard.covid19.data.gouv.fr/vue-d-ensemble?location=FRA)
 407 [ensemble?location=FRA](https://dashboard.covid19.data.gouv.fr/vue-d-ensemble?location=FRA); April 4th 2020), UK (www.nhs.uk/; April 9th 2020), Germany (corona.rki.de; April 2nd 2020),
 408 Spain (RTVE - Ministry of Health; www.rtve.es/noticias/20200415/mapa-del-coronavirus-espana/2004681.shtml; March
 409 31st 2020), Sweden (Public Health Agency of Sweden; [www.folkhalsomyndigheten.se/smittskydd-](https://www.folkhalsomyndigheten.se/smittskydd-beredskap/utbrott/aktuella-utbrott/covid-19)
 410 [beredskap/utbrott/aktuella-utbrott/covid-19](https://www.folkhalsomyndigheten.se/smittskydd-beredskap/utbrott/aktuella-utbrott/covid-19); April 13th 2020), Finland (National Institute for Health and Welfare THL;
 411 thl.fi/en/web/thlfi-en; April 7th 2020), Norway; data from the Norwegian Institute of Public Health;
 412 www.fhi.no/sv/smittsomme-sykdommer/corona/dags--og-ukerapporter/dags--og-ukerapporter-om-koronavirus).

3/21/2020

Number of cases: 50+ 25-49 10-24 < 10



A

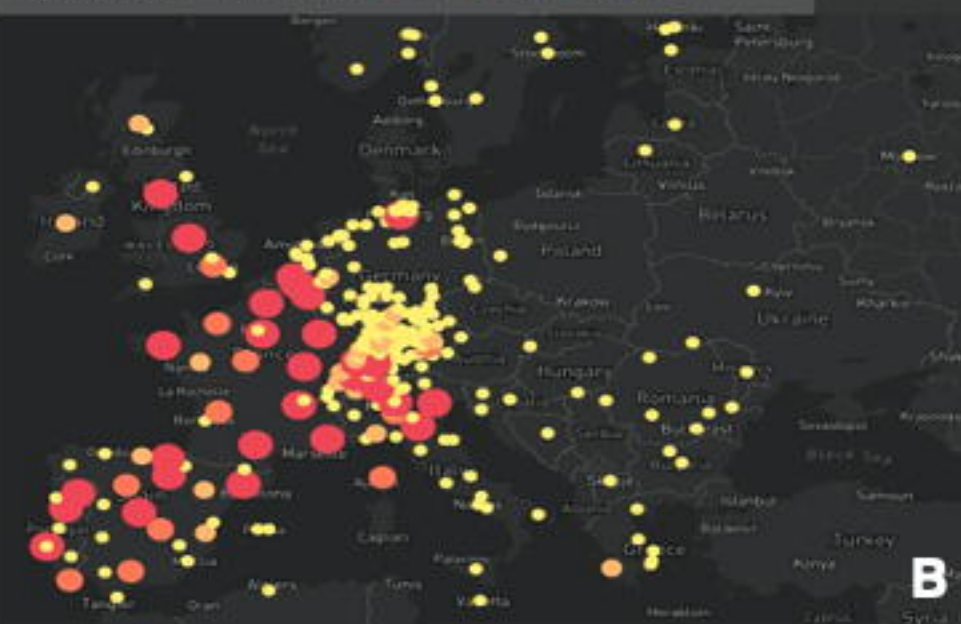
3/31/2020



C

3/21/2020

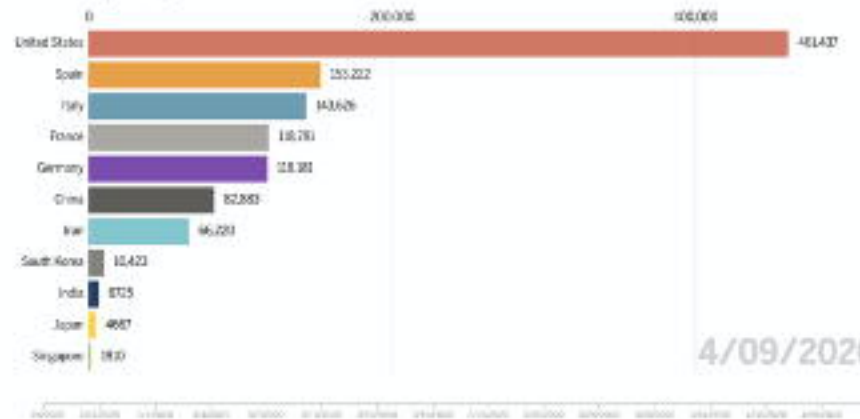
Number of cases: 50+ 25-49 10-24 < 10



B

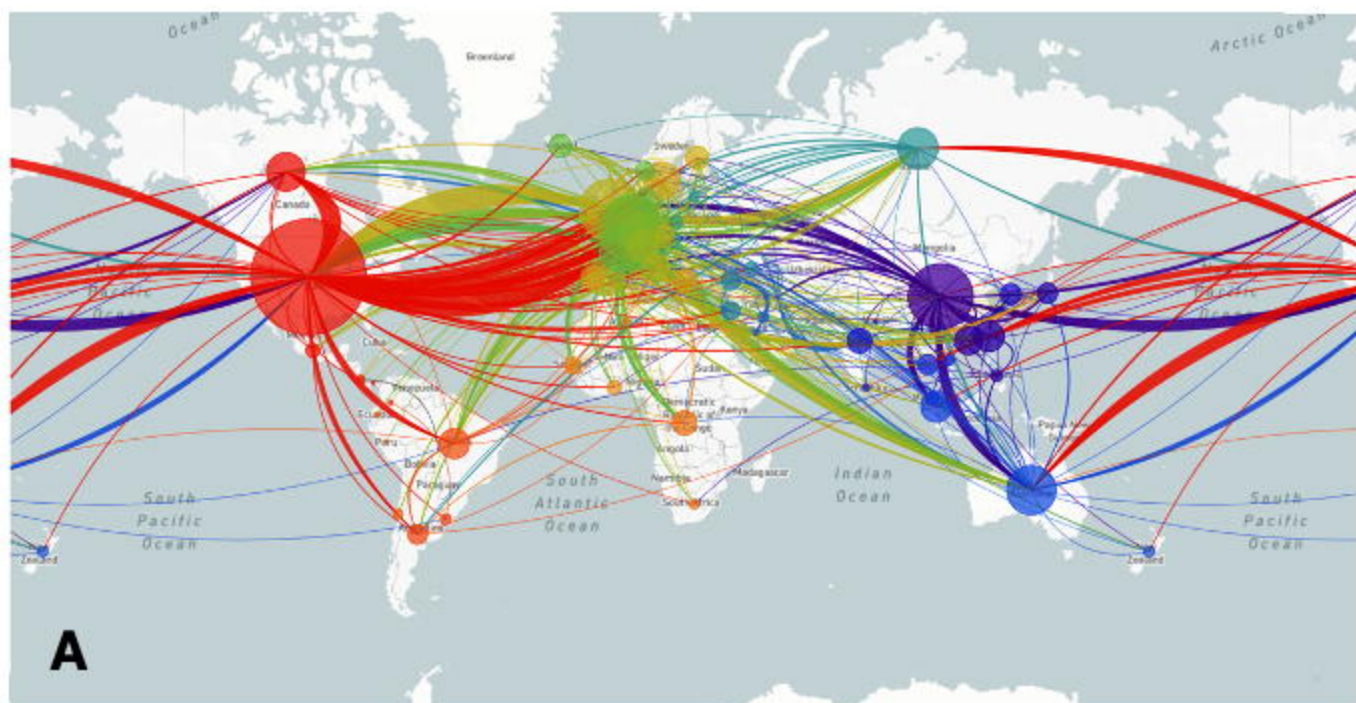
How coronavirus has spread around the world

Confirmed cases by country since Feb. 24

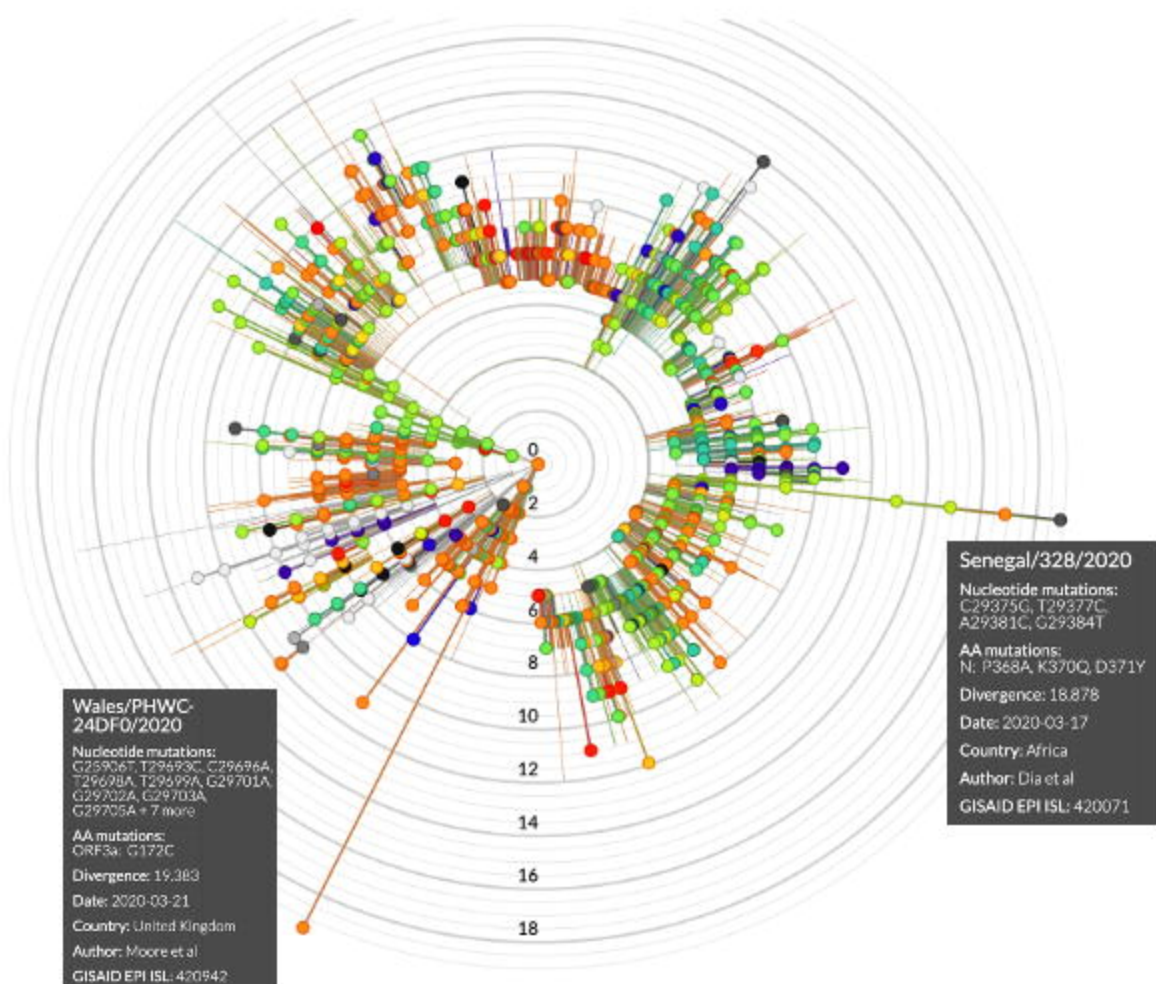


4/09/2020

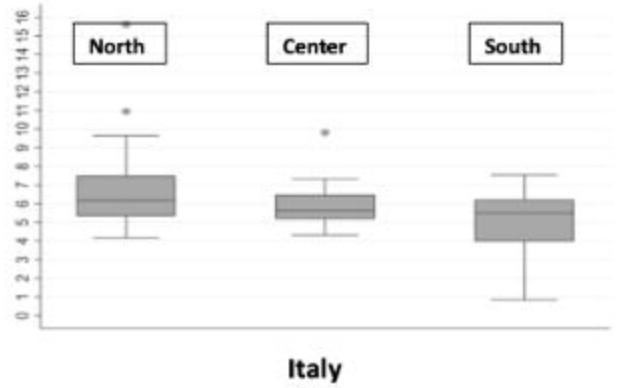
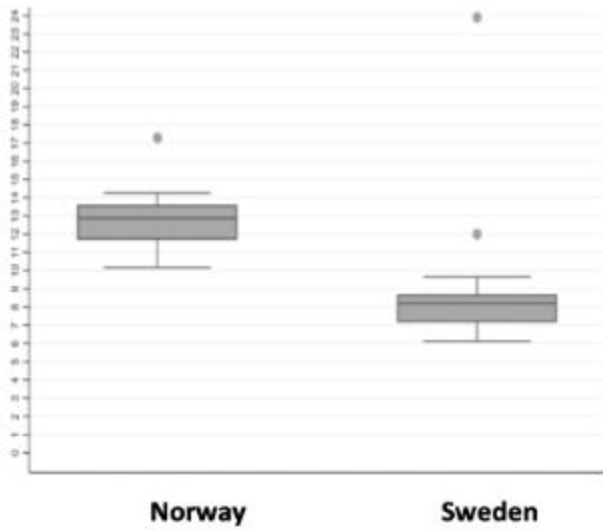
D



A



B



Region	Coef.	Std. Err.	t	P>t	[95% Conf. Interval]
intercept Northern Italy	6,63	0,33			5,97 7,29
Southern vs Northern Italy	-1,25	0,53	-2,35	0,02	-2,31 -0,20
Central vs Northern Italy	-0,76	0,55	-1,39	0,166	-1,84 0,32
Sweden vs Northern Italy	2,77	0,72	3,86	< 0.0001	1,35 4,19
Norway vs Northern Italy	6,32	0,77	8,25	< 0.0001	4,80 7,83

